Indian Journal of Radio & Space Physics
Vol. 4, March 1975, pp. 69-76

# Sporadic-E Formation due to Neutral Winds in the Equatorial Ionosphere

RATI DAHIYA, PRATIBHA VERMA & C. S. G. K. SETTY

Department of Physics & Astrophysics, University of Delhi, Delhi 110007

*Received 7 June* 1974

The ionization redistribution favouring the formation of thin Es layers due to neutral wind-shears has been investigated. The equations of motion for electrons and ions have been solved for the vertical velocity of ionization, taking into account the effect of the neutral wind velocity through the term containing the effective collision frequency. For simplicity, both electrons and ions have been assumed to be moving with the same velocity. The neutral wind velocity in the east-west direction has been assumed to be a sinusoidal function of the vertical height, where the wavelengths have been chosen empirically. Using the above velocity profiles for ionization, the continuity equation has been solved numerically using various input parameters such as the effective recombination coefficient, intensity of the electric field, and amplitude of the vertical velocity of ionization. It has, thus, been possible to generate theoretical models showing thin intense Es layers and models of vertical velocity profiles which can be compared favourably with those available from experimental results.

## 1. Introduction

THE NEUTRAL wind field (NWF) produces substantial changes in the E region ionization density profiles, thus coupling the chemical state to the dynamical state. The convergent motion of electrons and ions, giving rise to sporadic E, is most likely to be due to shears associated with horizontal winds in the neutral gas, as discussed by various workers. Axford[1] examined the structure of both the stationary and vertically moving layers, assuming a sinusoidal neutral wind profile. The numerical calculations, for 60-200 km altitude range showed that process of ion-convergence was very effective in the E region and weak in the D and F regions. He found that the wind-shear mechanism was most effective in the middle latitudes rather than at the equator or poles unless significantly non-horizontal wind-shears occurred. Axford and Cunnold[2] pointed out that the long-lived meteoritic ions must react strongly to the presence of wind-shears to form an Es layer. Chimonas and Axford[3] extended the wind-shear theory to take into account the effects associated with a neutral wind profile having a descending phase velocity. It was shown that the layers of long lived ions (presumably of meteoritic origin), formed at higher altitudes, were carried down with the wind profile to a region roughly 85-95 km in altitude, where they were dumped.

MacLeod[4] showed that the NWF can influence the distribution of ionization in the E region through mechanisms depending on the vertical shears of the neutral wind. The altitude of the overdense layers of ionization was also predicted using an equilibrium theory in which the ion motion was produced by a balancing of forces of neutral collisions and the geomagnetic field. Whitehead[5] has shown that the position of the electron density maxima relative to the horizontal winds must lie in certain height ranges irrespective of the electric fields or wind profile movements, provided these are steady. Recently, Reddy and Devasia[6] have shown that the horizontal shears of horizontal neutral winds are the most likely sources of the blanketing Es layers observed at the magnetic equator. The horizontal wind-shears of the required magnitude are shown to be provided by the internal gravity waves of short period.

The purpose of this paper is to develop a theoretical model for the formation of the equatorial sporadic E layer on the basis of the wind-shear mechamism. A similar model was reported in our earlier paper[7] where the effect of the neutral winds was not considered. In the present paper, the equation of motion for the ionized particles has been solved, taking into account the effect of electric fields, Lorentz force and the ion-drag due to the neutral particle velocity. A time-dependent solution of the continuity equation has been found with the help of a computer simulation experiment. The exact process, how an Es layer starts building up before a steady solution for the electron density is reached, has clearly been shown. Keneshea and MacLeod[8] have also described the evolution of the physical state of the ionosphere as the time dependent solution to a set of coupled partial differential equations involving the dynamics, thermodynamic and electromagnetic variables.

## 2. Theory

When the ionosphere is not at rest, and the source of the altitude variations in ion density is to be found in the divergence terms, we have the continuity equations as

$$\frac{\partial n_i}{\partial t} = q_i - L_i - \nabla \cdot (n_i \mathbf{V}_i) \qquad \ldots(1)$$

where $q_i$ and $L_i$ are the production and loss terms of the $i$th species, $n_i$ is the number density of the same species and $\mathbf{V}_i$ represents the velocity of ionization of that species.

The appearance of the divergence terms in the continuity equations produces the following effects :

(i) Coupling of the equations of motion (determing ($\mathbf{V}_i$) with the equations of continuity.

(ii) Coupling of the number densities at different altitudes through the spatial derivatives in Eq. (1) and an indirect change in the effect of reaction terms on $\partial n_i/\partial t$ resulting from the change brought in $n_i$ through the divergence terms.

The first effect may include a further coupling with the neutral equations of motion and Maxwell's equations, depending on what forces are dominant in determining the ion velocities. In the present calculations the ion velocities have been derived from the neutral wind profile using the electromagnetic collision equilibrium process.

### 2.1 Basic Equations

The equations of motion for singly charged ions and electrons are respectively[9]

$$n_i m_i \left\{ \frac{\partial}{\partial t} + \mathbf{V}_i \cdot \nabla \right\} \mathbf{V}_i = n_i e (\mathbf{E} + \mathbf{V}_i \times \mathbf{B}) + n_i m_i \nu_{in} (\mathbf{U} - \mathbf{V}_i) \qquad \ldots(2)$$

$$n_e m_e \left\{ \frac{\partial}{\partial t} + \mathbf{V}_e \cdot \nabla \right\} \mathbf{V}_e = -n_e e (\mathbf{E} + \mathbf{V}_e \times \mathbf{B}) + n_e m_e \nu_{en} (\mathbf{U} - \mathbf{V}_e) \qquad \ldots(3)$$

where $e$ is the magnitude of the electron charge; $\mathbf{E}$, the electric field intensity; $\mathbf{B}$, the magnetic induction; $\mathbf{U}$, the neutral wind velocity; $n_e$, the electron density; $n_i$, the ion density; $\nu_{in}$, the collision frequency between ions and neutrals; and $\nu_{en}$ is collision frequency between electrons and neutrals; $m_i$, $m_e$ the ion and electron mass; and $\mathbf{V}_i$, $\mathbf{V}_e$ the velocity of ions and the electrons, respectively.

From Eq. (1) the continuity equations for ions and electrons respectively can be written as

$$\frac{\partial n_i}{\partial t} + \nabla \cdot (n_i \mathbf{V}_i) = q_i - \alpha_i n_i n_e \qquad \ldots(4)$$

$$\frac{\partial n_e}{\partial t} + \nabla \cdot (n_e \mathbf{V}_e) = \sum_i q_i - \left(\sum_i \alpha_i n_i\right) n_e \qquad \ldots(5)$$

where $\alpha_i$ is the ion-electron recombination coefficient.

A Cartesian coordinate system ($X$, $Y$, $Z$) has been used such that the $XY$-plane is horizontal, $X$ is directed magnetically northward, $Y$, westward and $Z$, vertically upward. The ionosphere has been assumed to be plane and horizontally stratified.

The components of the vector quantities are taken as

$$\left.\begin{array}{ll} \mathbf{B} = B_0 (X, 0, Z) & X^2 + Z^2 = 1 \\ \mathbf{E} = (E_x, E_y, E_z) & \mathbf{V}_i = (V_{xi}, V_{yi}, V_{zi}) \\ \mathbf{U} = (U_x, U_y, U_z) & \mathbf{V}_e = (V_{xe}, V_{ye}, V_{ze}) \end{array}\right\} \qquad \ldots(6)$$

As the Es layers are usually thin in the vertical direction ($\sim$1 km) compared with their typical horizontal dimensions ($\sim$100 km), we can take,

$$\frac{\partial}{\partial x} = \frac{\partial}{\partial y} = 0 \text{ and } \frac{\partial}{\partial z} = \frac{d}{dz} \qquad \ldots(7)$$

Also, since the duration of the layers is often sufficiently long ($\sim 10^4$ sec) in comparison to the time of formation ($\sim 10^3$ sec), a steady-state solution of $\mathbf{V}_i$ may be assumed.

As a result of these assumptions,

$E_x$, $E_y$ and $B_0$ are all constants.

The inertial terms on the left side of Eqs. (2) and (3) can also be neglected because the time scales characterizing inertial effects are much greater than the mean collision interval with neutrals and the gyro-periods of the charged particles. Thus, these equations become

$$\frac{\mathbf{E}}{B_0} + \left[\frac{\mathbf{V}_i \times \mathbf{B}}{B_0}\right] + R_i (\mathbf{U} - \mathbf{V}_i) = 0 \qquad \ldots(8)$$

$$-\frac{\mathbf{E}}{B_0} - \left[\frac{\mathbf{V}_e \times \mathbf{B}}{B_0}\right] + R_e (\mathbf{U} - \mathbf{V}_e) = 0 \qquad \ldots(9)$$

where

$$R_i = \frac{m_i \nu_{in}}{eB_0} = \frac{\nu_{in}}{\omega_i}, \; R_e = \frac{m_e \nu_{en}}{eB_0} = \frac{\nu_{en}}{\omega_e} \qquad \ldots(10)$$

At the height of 100 km and $R_i \approx 10$ and $R_e \approx 0{\cdot}003$ (Axford[1]),

Assuming $n_i = n_e$, $V_{zi} \approx V_{ze}$ ($= V_z$) and $R_e \ll R_i$, and solving for $V_{zi}$, we get

$$V_{zi} = V_z = -\frac{R_i^2 + Z^2}{\Delta_i}\left[-\left(\frac{R_i^2 XZ}{R_i^2 + Z^2} + \frac{R_e XZ}{R_{e2}^2 + Z}\right)U_x + \left(\frac{R_i^2 X}{R_i^2 + Z^2} - \frac{R_e^2 X}{R_e^2 + Z^2}\right) U_y - (R_e + R_i) U_z - \left(\frac{XZ}{R_i^2 + Z^2} - \frac{XZ}{R_e^2 + Z^2}\right)\frac{E_z}{B_0} + \left(\frac{XR_i}{R_i^2 + Z^2} + \frac{XR_e}{R_e^2 + Z^2}\right)\frac{E_y}{B_0}\right] \qquad \ldots(11)$$

where, $\Delta_i = -R_i (R_i^2 + 1)$ ...(12)

and $V_i$ represents the vertical velocity of ionization.

## 3. Numerical Computations

The vertical velocity of ionization, $V_z$, has been computed in steps of 1 km from 90 to 150 km altitude, using Fq. (11). The values of the dip angle range from 0 to 10° and the same is the range for the angle between the electric intensity and due east. The electron collision frequencies have been taken from the model given by Setty[10] and the ion collision frequencies have been interpolated graphically at 1 km intervals from Sugiura and Cain[11]. The gyro-frequencies of electrons and ions have values $7{\cdot}05 \times 10^6$ and 143 rad $sec^{-1}$, respectively, which correspond to a magnetic flux density of $4 \times 10^{-5}$ Wb $m^{-2}$ (40,000 $\gamma$) and a molecular weight of 29 for the ions.

The north-south and vertical components of the neutral wind velocity have been neglected and the effect of the neutral wind has been accounted for through the east-west component only. It is assumed to be a sinusoidal function of vertical height; $U_y = U_0 \sin(2\pi Z_0/\lambda)$ where $U_0$ is the maximum amplitude of the neutral wind velocity, $Z_0$ $(= H - 90$ km) is the reduced height and $\lambda$ is the vertical wavelength. For comparison, $U_0$ has been assigned two values 100 and 50 m $sec^{-1}$ (Axford *et al.*[9], Richmond[12]) corresponding to the E region winds. For the vertical wavelength Axford[1] adopted the values as $\lambda = 5$, 10, 12 and 50 km at the heights of 85, 120, 145 and 230 km, respectively. Zimmerman[13] stated that the smallest vertical wavelengths varied from 2 km at 100 km to 12 km at 120 km altitudes. Also Wright *et al.*[14] observed an increase in vertical wavelength with height. Considering these results and after properly scrutinizing the wind data published from World Data Centre A, we have chosen two sets of wavelengths one as $\lambda = 6$ km up to 110 km and 40 km above 110 km, and another as $\lambda = 12$ km up to 110 km. and 50 km above 110 km. The electric field intensity is assumed to have 3 values as 1·0, 2·0 and 2·6 mV/m. The other two values are comparatively high though Closs[15] has used an electric intensity of 2 mV/m and Suguira and Cain[11] have adopted an electric field of 2·4 mV/m. Comparative study is made by taking the recombination coefficient as $10^{-8}$, $3 \times 10^{-8}$ (MacLeod[16]), $10^{-9}$ (Reddy and Devasia[6]), and $10^{-11}$ $cm^3$ $sec^{-1}$, respectively. The latter two values correspond to the metallic ions because minor constituents such as meteoritic ions $Mg^+$, $Fe^+$ and $Si^+$ have recombination coefficients as small as $10^{-12}$ $cm^3$ $sec^{-1}$.

The continuity Eq. (1) in the form

$$\frac{\partial n}{\partial t} = q - \alpha n^2 - \frac{d}{dz}(nV_z) \qquad ...(13)$$

has been solved numerically to compute the electron density and to see if a layer of enhanced ionization forms. In Eq. (13) $q = \alpha n_0^2$ where $n_0$ is the electron density in the absence of $V_z$ and it is assumed to have a Chapman distribution.

$$n_0 = n_{mo} \exp \tfrac{1}{2} [1 - Z - \sec \chi \exp(-Z)] \qquad ...(14)$$

where $n_{mo}$ is the maximum electron density at the peak of the layer and $Z = (H - H_m)/H_s$, $H_m$ being the height of the peak of the Chapman layer and $H_s$ the scale height.

The above parameters have been given the numerical values as $n_{mo} = 2{\cdot}0 \times 10^5$ $cm^{-3}$, $H_m = 110$ km, $\chi = 0°$ and $H_s = 7{\cdot}5$ km, The electron densities have been computed for different intervals of time and it is seen that the electron density distribution reaches a stationary state after about 2400 seconds as discussed in Sec. 4.

## 4. Results and Discussion

The vertical velocity of ionization has been computed taking different sets of $\alpha$, $E$, $U_0$ and, $\lambda$, for $I$ and $\theta$ varying from 1 to 10°. Fig. 1 is a plot of the vertical velocity versus height for $\lambda = 6$ km up to 110 km and 40 km above this altitude. It is clear from Fig. 1 that the vertical velocities of ionization vary appreciably with height. For the whole range of $\theta$, we notice a clear sinusoidal variation of $V_z$ and the velocity gradient becomes negative at many points favouring the occurrence of Es layer. It is seen that at lower altitudes (below 110 km) the velocities are approximately same for all the values of $\theta$ but at higher altitudes (above 110 km), the velocities decrease as $\theta$ increases. The vertical velocities calculated for other values of $\alpha$, $E$, $U_0$ and $\lambda$ also show similar variations but their magnitudes are different.

Fig. 2 is a plot of $V_z$ against height for a constant electric field orientation ($\theta = 2°$) and different values of $I$. It is seen that as the dip angle increases from 2 to 10°, the $V_z$ values move towards the negative side at lower altitudes (90-115 km) and towards the positive side at higher altitudes (above 115 km). For $I \geqslant 8°$, the velocities do not change significantly and the values of $V_z$ for $I = 8°$ and $I = 10°$ overlap. Similar variations are obtained for other values of the parameters $\alpha$, $E$, $U_0$ and $\lambda$.

In order to examine the behaviour of the velocity gradient, $-(dV_z/dZ)_{max}$ is plotted against $\theta$ for different values of $I$. One representative curve corresponding to the parameters of Fig. 1 is shown in Fig. 3. It is seen that $-(dV_z/dZ)_{max}$ increases linearly with $\theta$ at all dip angles and the rate of increase of the gradient (represented by the slope) is more at lower dip angles. Fig. 4 is a plot of $-(dV_z/dZ)_{max}$ against $I$ for different values of $\theta$. It is seen from Fig. 4 that

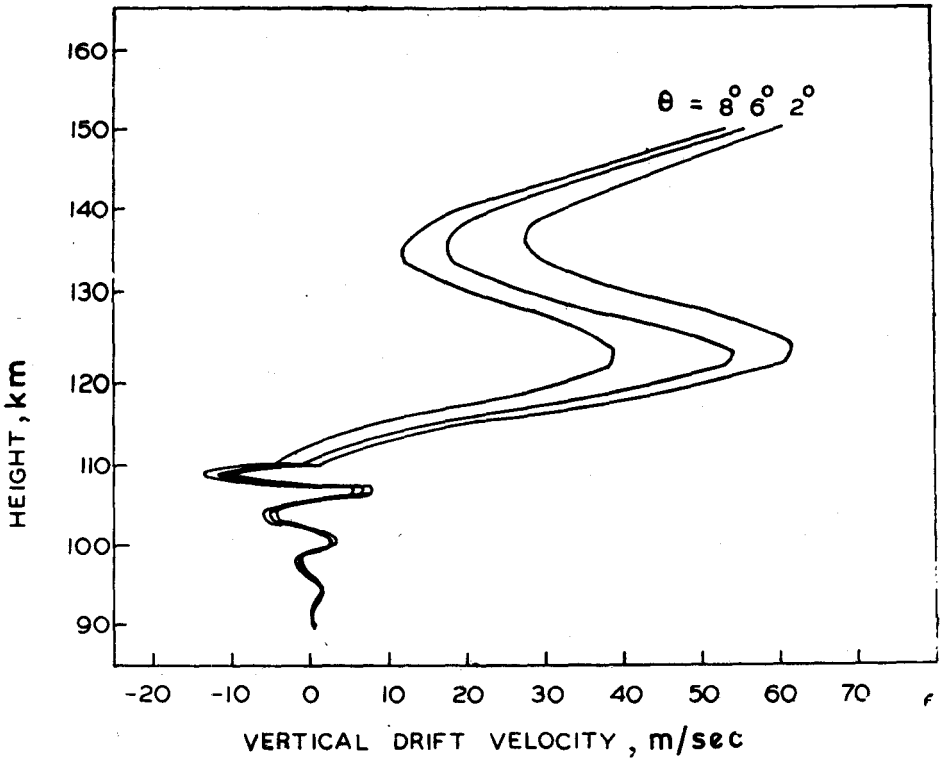


Fig. 1 — Plot of $V_z$ versus height for a constant dip angle ($I = 8°$) for different values of $\theta$ [$U_0$ = 100 m sec$^{-1}$, $\lambda$ = 6 km below and 40 km above 110 km height, $E$ = 2·6 mV m$^{-1}$]

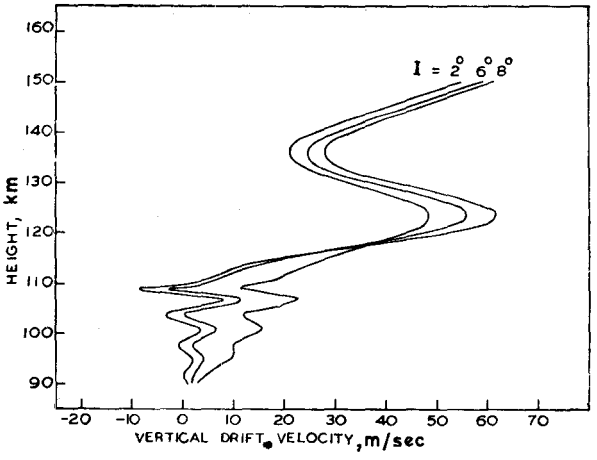


Fig. 2—Plot of $V_z$ versus height for a constant orientation of the electric field ($\theta = 2°$) for different values of $I$ [Parameters used are same as in Fig. 1]

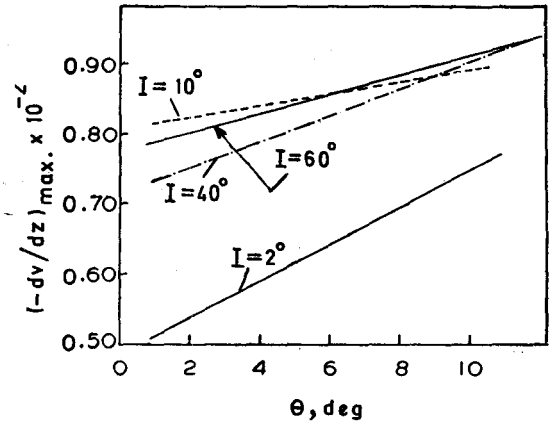


Fig.3 —Plot of gradient of the vertical velocity, $-(dV_z/dZ)_{max}$, as a function of $\theta$ [Parameters used are as given in Fig. 1]

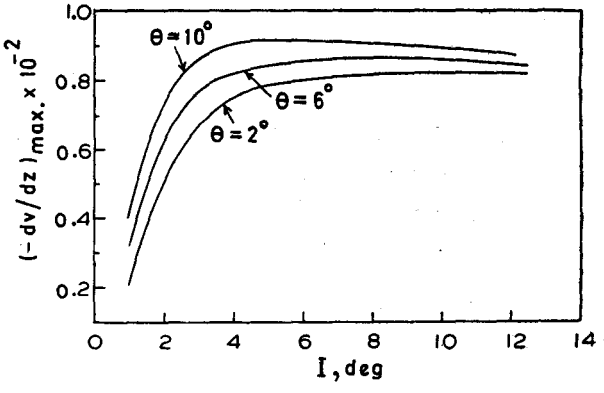


Fig. 4—Plot of gradient of the vertical velocity, $-(dV_z/dZ)_{max}$, as a function of $I$ [Parameters used are as in Fig. 1]

as $I$ increases, the gradient shows a steep rise and attains a peak value at $I = 6°$, followed by a decline as $I$ increases further.

In order to see the effect of neutral winds on the formation of Es layer near the magnetic equator, the continuity Eq. (13) has been solved using the ionization drift velocities calculated as above. The electron density profiles have been computed at certain intervals of time for different sets of parameters $\alpha$, $E$, $U_0$ and $\lambda$. These electron density profiles have been plotted in Figs. 5-9 for $t = 0$, 300 and 2400 sec. It is seen that as soon as the vertical drift velocity is introduced, the Chapman electron density distribution changes and peaks of electron density grow wherever the vertical velocity gradient has a maximum negative value (not necessarily at $V_z = 0$). The peaks grow with time and a stationary state is arrived at

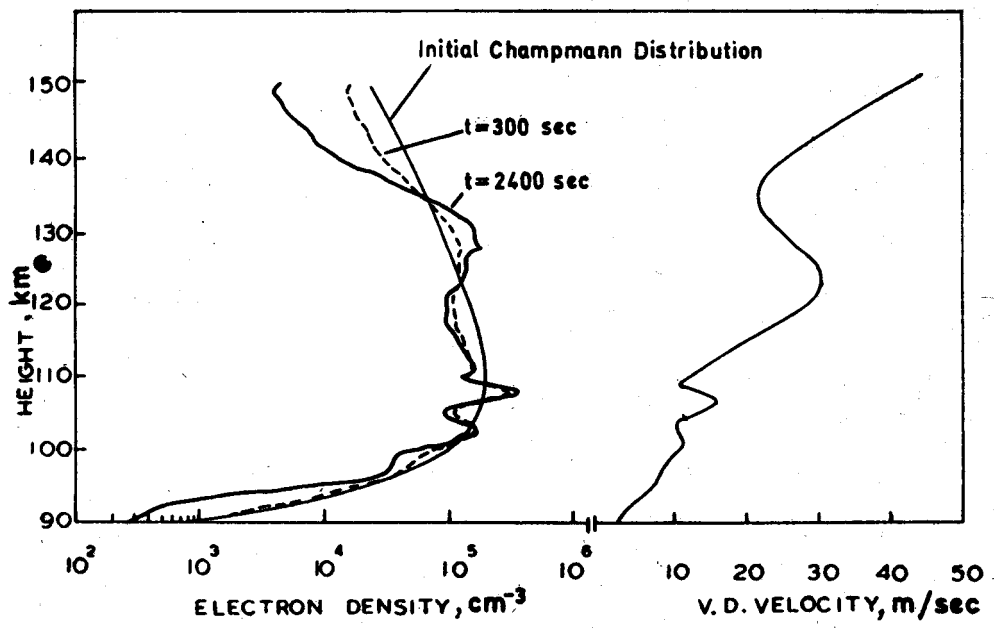


Fig. 5—Computed electron density profiles and the corresponding vertical drift velocity [Parameter used are: $I = 2°, \theta = 2°, \alpha = 10^{-8}$ cm$^3$ sec$^{-1}$, $E = 2{\cdot}0$ mV m$^{-1}$, $U_0 = 50$ m sec$^{-1}$, and $\lambda$=6 km below and 40 km above 110 km altitudes]

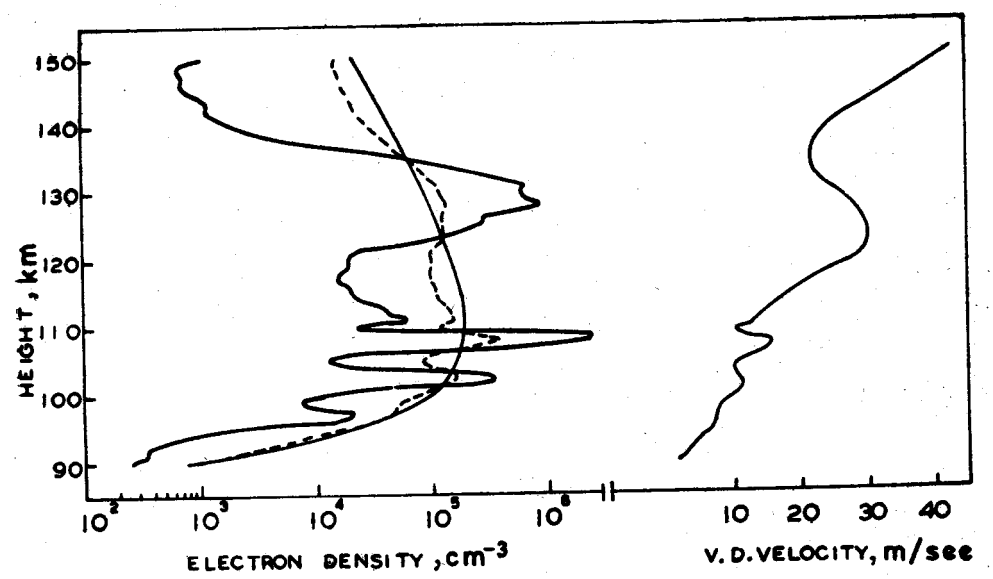


Fig. 6—Same as Fig. 5 [Parameters used are same as in Fig. 5 except $\alpha = 10^{-9}$ cm$^3$ sec$^{-1}$]

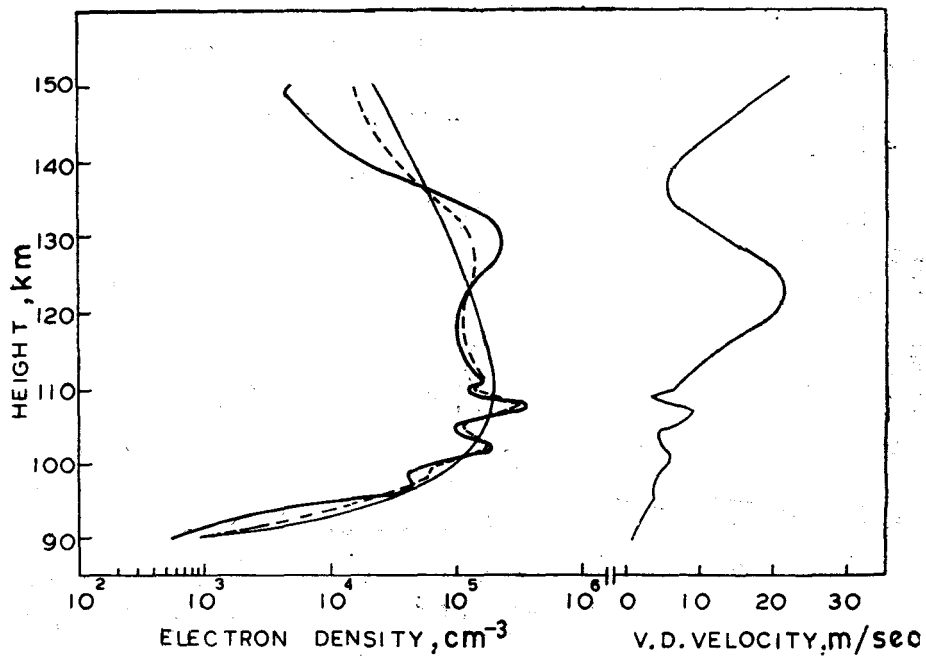


Fig. 7—Same as Fig. 5 [Parameters used are same as in Fig. 5 except $E = 1{\cdot}0$ mV m$^{-1}$]

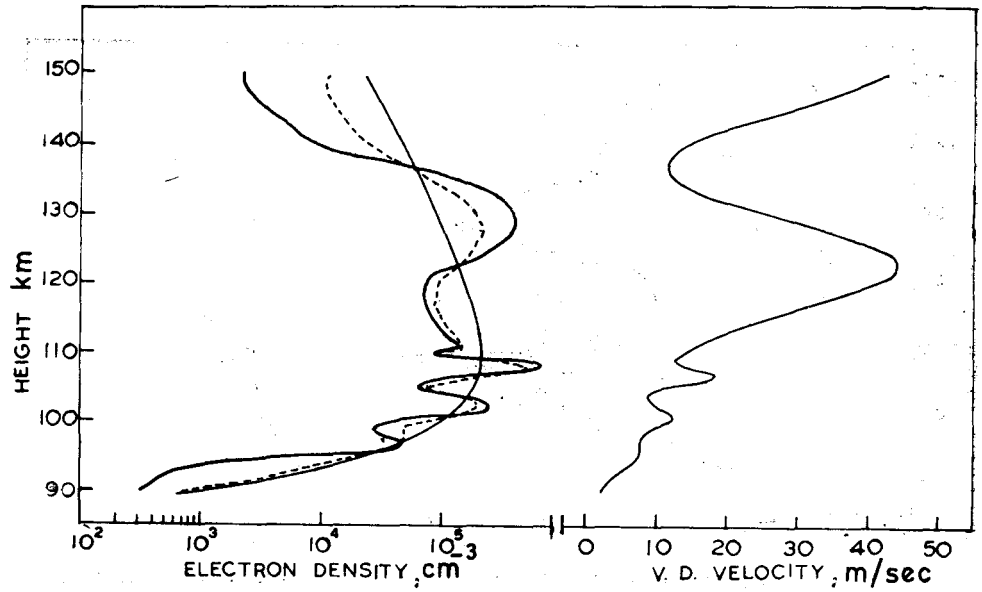


Fig. 8—Same as Fig. 5 [Parameters used are same as in Fig. 5 except $U_0 = 100$ m sec$^{-1}$]

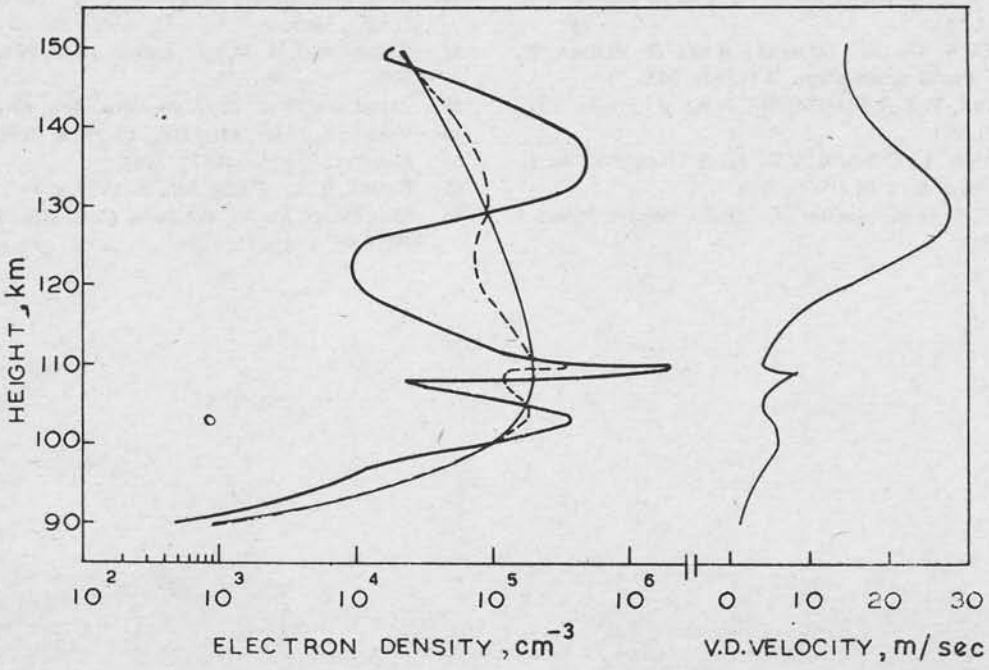


Fig. 9—Same as Fig. 5 [Parameters used are same as in Fig. 5 except $E$=1·0 mV m$^{-1}$ and $\lambda$ = 12 km below and 50 km above 110 km altitude]

approximately $t$ = 2400 sec. By examining these figures, the following points are noted :

(i) From Figs. 5 and 6, it is seen that the effect of decreasing $\alpha$ is to increase the peak electron density of the Es layer substantially.

(ii) The effect of the electric field, which can be seen by comparing Figs. 5 and 7, is not so pronounced as that of $\alpha$. However, there is increase in the peak electron density with the increase in the electric field.

(iii) Similarly Figs. 5 and 8 show clearly that the amplitude of the vertical velocity plays an important role in determining the peak electron density and the vertical velocity profiles. An increase in $U_0$ increases both $-(dV_z/dZ)_{max}$ and the peak electron density.

(iv) The vertical wavelength of the neutral wind velocity is the most important parameter which determines the number of Es layers and their heights, the peak electron concentration and the thickness of the layers. However, the most prominent Es layer is usually the uppermost near 108 km altitude. From Figs. 7 and 9 it is seen that the number of layers and their peak electron density increase with increase in $\lambda$, whereas the thickness of the layers decreases.

In this context it may also be pointed out (not shown in figures) that the effect of $I$ is to increase the peak electron density for $I \leqslant 6°$. This behaviour may be expected from Fig. 4 which shows that the velocity gradient is the maximum near $I = 6°$ and remains nearly constant for $I > 6°$.

On the basis of ionograms taken at Thumba (dip $\sim$ 0·6°S), Reddy and Devasia[6] have shown that the height at which the Es layers occur during daytime ranges from 95 to 105 km in more than 90% of the cases. Their experimental values for the blanketing Es layers are very much in agreement with our theoretically calculated electron density profiles Fig. 3 of these workers[6] shows the occurrence of multiple Es layers between 100 and 110 km altitude which is also favoured by our electron density profiles.

**Acknowledgement**

The work reported in this paper was carried out under the research scheme 'Studies of the Ionosphere' supported by the University Grants Commission, New Delhi. One of the authors (R. D.) is indebted to the CSIR, New Delhi, for a fellowship. The authors would like to thank Dr B. C. N. Rao of National Physical Laboratory, New Delhi, for helpful discussions.

**References**

1. AXFORD, W. I., *J. geophys. Res.*, **68** (1963), 769.
2. AXFORD, W. I. & CUNNOLD, D. M., *Radio. Sci.*, **1** (1966), 191.
3. CHIMONAS, G. & AXFORD, W. I., *J. geophys. Res.*, **73** (1968), 111.
4. MACLEOD, M. A., *Meteorol. Monographs.*, **9** (1968), 139.
5. WHITEHEAD, J. D., *Radio. Sci.*, **7** (1972), 425.

6. REDDY, C. A. & DEVASIA, C. V., *Planet. Space Sci.*, **21** (1973), 811.
7. SETTY, C. S. G. K., DAHIYA, RATI & VERMA, P., *Indian J. Radio Space Phys.*, **3** (1974), 263.
8. KENESHEA, T. J. & MACLEOD, M. A., *J. atmos. Sci.*, 27 (1970), 981.
9. AXFORD, W. I., CUNNOLD, D. M. & GLEESON, L. J., *Planet. Space Sci.*, **14** (1966), 909.
10. SETTY, C. S. G. K, *Indian J. Radio Space Phys.*, **1** (1972), 38.
11. SUGUIRA, M. & CAIN, J. C., *J. geophys. Res.*, **71** (1966), 1869.
12. RICHMOND, A. D., *J. atmos. terr. Phys.*, **35** (1973), 1083.
13. ZIMMERMAN, S. P., *J. geophys. Res.*, **69** (1963), 784.
14. WRIGHT, J. W., MURPHY, C. H. & BULL, G. V., *J. geophys. Res.* **72** (1967), 1443.
15. CLOSS, R. L., *Radio Sci.*, **6** (1971), 939.
16. MACLEOD, M. A., *Air Force Cambridge Res. Lac. Rept. WSTSE*, **1** (1964).